Applied Physics Letters

GaSb diode lasers tunable around 2.6 μm using silicon photonics resonators or external diffractive gratings

Cite as: Appl. Phys. Lett. **116**, 081105 (2020); https://doi.org/10.1063/1.5140062
Submitted: 25 November 2019 . Accepted: 15 February 2020 . Published Online: 27 February 2020

S.-P. Ojanen, J. Viheriälä, M. Cherchi, N. Zia, E. Koivusalo, P. Karioja, and M. Guina

Applied Physics Letters ARTICLE scitation.org/journal/apl

GaSb diode lasers tunable around 2.6 μm using silicon photonics resonators or external diffractive gratings

Cite as: Appl. Phys. Lett. **116**, 081105 (2020); doi: 10.1063/1.5140062
Submitted: 25 November 2019 · Accepted: 15 February 2020 ·
Published Online: 27 February 2020

S.-P. Ojanen,[1,a)] J. Viheriälä,[1] M. Cherchi,[2] N. Zia,[1] E. Koivusalo,[1] P. Karioja,[3] and M. Guina[1]

AFFILIATIONS

[1]Optoelectronics Research Centre, Tampere University, Tampere FI-33720, Finland
[2]VTT Technical Research Centre of Finland, Espoo FI-02044, Finland
[3]VTT Technical Research Centre of Finland, Oulu FI-90570, Finland

[a)]Author to whom correspondence should be addressed: samu-pekka.ojanen@tuni.fi

ABSTRACT

We report two tunable diode laser configurations emitting around 2.6 μm, where the gain is provided by a high-gain GaSb-based reflective semiconductor optical amplifier. The lasers are driven in pulsed mode at 20 °C, with a pulse width of 1 μs and 10% duty cycle to minimize heating effects. To demonstrate the broad tuning and high output power capability of the gain chip, an external cavity diode laser configuration based on using a ruled diffraction grating in a Littrow configuration is demonstrated. The laser shows a wide tuning range of 154 nm and a maximum average output power on the order of 10 mW at 2.63 μm, corresponding to a peak power of 100 mW. For a more compact and robust integrated configuration, we consider an extended-cavity laser design where the feedback is provided by a silicon photonics chip acting as a reflector. In particular, the integrated tuning mechanism is based on utilizing the Vernier effect between two thermally tunable micro-ring resonators. In this case, a tuning range of around 70 nm is demonstrated in a compact architecture, with an average power of 1 mW, corresponding to a peak power of 10 mW.

Many industrial and environment-related applications require monitoring multiple gases, including H_2S, C_2H_4, CH_4, CO, CO_2, and N_2O, which all exhibit strong absorption lines in the 2–3.5 μm wavelength region.[1] To this end, the development of specialized light sources to be used for spectroscopic analysis in this wavelength range has attracted increased attention.[2–5] However, available light sources addressing this need do not offer a suitable combination of output power, spectral coverage, compactness, power consumption, and price.[6–8]

Tunable external or extended cavity lasers, which combine a semiconductor gain chip and an external feedback and tuning mechanism, present an attractive option for the spectroscopic applications, enabling a wide tuning range and a narrow linewidth simultaneously.[9,10] This is in contrast to monolithic diode lasers, such as vertical cavity surface emitting lasers (VCSELs) and distributed feedback (DFB) lasers,[11,12] where a compromise has to be made for at least one of these characteristics. On the other hand, traditional external cavity lasers have a larger footprint and increased cost. These aspects can be mitigated by developing an integrated solution exploiting silicon photonics. Such solutions have been widely adopted for III–V/silicon photonic integration at telecommunication wavelengths and are gradually breaking ground to wavelengths longer than 2 μm.[3,5,13]

For a III–V active element, GaSb-based type-I quantum well (QW) heterostructures are ideal to be used as gain elements in tunable diode lasers (TDLs) for the 2–3 μm range, as they can access the entire range with simple direct electrical injection.[14] However, their deployment in tunable laser architectures has seen little development, in particular, at wavelengths beyond 2.3 μm where non-radiative recombination processes limit the output power and temperature operation range.[15,16] This difficulty is, for example, reflected when comparing the power levels of state-of-the-art GaSb-based type-I superluminescent diodes (SLDs). An output power as high as 120 mW is attained near 2 μm at room temperature (RT),[17] while the power drops by two orders of magnitude to the mW-level when translating to 2.55 μm.[18] Recently, type-I GaSb-based tunable external cavity diode lasers (ECDLs), with feedback provided by first-order diffraction from a grating, have been demonstrated around the 2.0–2.4 μm wavelength range. In one configuration, the grating was used as the end

mirror in the laser cavity, and tunability was obtained by rotating the grating (Littrow configuration). This laser demonstrated less than 5 mW of continuous wave (CW) output power at 20 °C, with a tuning range of less than 100 nm per chip.[19] In another configuration, the first order diffraction was directed to an end mirror, and tunability was obtained by rotating the mirror (Littman–Metcalf configuration). This laser demonstrated a CW output power of over 20 mW at 20 °C, with a wide tuning range of up to around 300 nm.[20] For integrated hybrid lasers, a tunable type-II quantum well III–V-on-silicon laser operating near 2.35 μm wavelength has recently been demonstrated with mW-level peak power near RT, and the platform is able to accommodate lasers up to 2.5 μm wavelength maximum.[13] So far, integrated light sources in the wavelength range of 2.5–2.7 μm have seen little development. However, gases such as H_2O and H_2S exhibit strong absorption in this range,[1] which would make such light sources important in many sensing applications, such as measuring humidity.

We report two TDL configurations around 2.6 μm: (a) a Littrow laser and (b) an extended cavity laser that utilizes a silicon photonic (SiPh) reflector chip exploiting the Vernier effect between two micro-ring resonators (MRRs) (Vernier laser). For the SiPh implementation, we tested two coupling schemes: (1) output taken either from the facet of the gain chip or (2) the end-facet of the SiPh waveguide. In each laser configuration, we utilized reflective semiconductor optical amplifiers (RSOAs) to provide double-pass gain and cavity feedback. The epitaxial structure of the gain chip consisted of two compressively strained GaInAsSb QWs (~2% strain) positioned within two 270 nm thick lattice-matched AlGaAsSb waveguide layers. The active region was embedded in 2 μm thick p- and n-AlGaAsSb cladding layers. In order to minimize the free carrier absorption near the active region, the doping levels in the cladding were linearly graded from 2×10^{17} cm^{-3} to 2×10^{18} cm^{-3}.

The geometry of the gain chip employed a "J-shape" waveguide layout, where the front facet of the ridge waveguide (RWG) is tilted to reduce back reflections and the rear facet is kept straight to provide maximum reflection. The RWG bend follows an Euler spiral geometry,[21] where the bending radius decreases with the increasing arc length. A large minimum bending radius of 18 mm was used in the RSOAs, leading to negligible bending losses. The tilt angle at the front facet was 7°, minimizing the back reflections, and the length of the device was 2.85 mm. A schematic of the RSOA is shown in Fig. 1.

The RSOAs were mounted p-side up on AlN submount for the Littrow laser, for the ease of fabrication, and p-side down for the Vernier laser, for compatibility with the input channel in the SiPh chip. Both chips had an anti-reflection coating (ARC) on the front facet to maximize output coupling. The rear facet was high-reflectance coated (HRC) to minimize mirror losses for the p-side down chip and left as-cleaved for the p-side up mounted chip, providing ~30% reflectance. All tests presented in this paper were performed in pulsed operation at 20 °C, with a pulse width (PW) of 1 μs and 10% duty cycle (DC). The power measurements were averaged over time and are

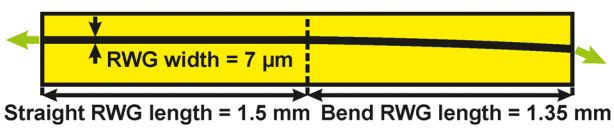

FIG. 1. Schematic of the RSOA chip.

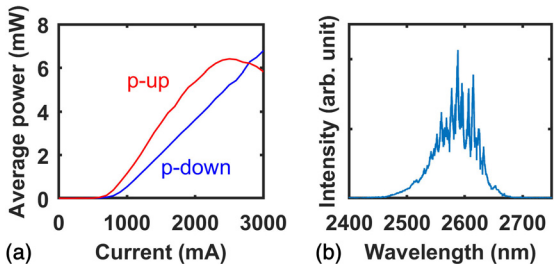

FIG. 2. (a) The average output power of the p-side up mounted (red) and p-side down mounted (blue) RSOA as a function of injection current pulse amplitude and (b) the emission spectrum of the RSOA chip.

hereafter referred to as average powers, unless otherwise mentioned. Figure 2 (a) shows the measured average output power of the RSOA as a function of pulse amplitude for the p-up mounted chip (red) and the p-down mounted chip (blue), and Fig. 2(b) shows the measured output spectrum. The devices exhibited maximum average output powers of 6.4 mW and 6.8 mW, corresponding to peak powers of 64 mW and 68 mW, for the p-up mounted chip and the p-down mounted chip, respectively. The full width at half maximum (FWHM) of the spectrum is 84 nm. Further improvement in average power can be obtained by optimizing the pulsed injection parameters.[18]

In the Littrow laser, the RSOA was placed on a heatsink, and the beam from the front facet with the bent WG was coupled into an external ruled reflective diffraction grating with an aspheric lens. The diffraction grating provides feedback into the RSOA at the first diffraction angle. The grating was rotated around a pivot point in order to minimize mode hopping, as defined in Ref. 10. Because the output beam from the grating moves as the grating is rotated, the output was coupled to a multimode fiber (MMF) from the rear facet of the RSOA. The MMF was intentionally brought in at an angle in order to minimize the parasitic feedback from the fiber tip, at the expense of attaining a weaker signal. A schematic of the Littrow laser is shown in Fig. 3.

The gain chip was then driven with 700 mA pulses, and the output spectrum was scanned as a function of the angle of the diffraction grating, using a Fourier transform infrared (FTIR) spectrometer. Figure 4(a) shows the emission wavelength of the laser as a function of the motorized actuator position, which corresponds to the angle of the diffraction grating. The laser exhibited a wide tuning range of 154 nm, emitting at wavelengths from 2513 nm to 2667 nm. Even with the rotation around the pivot point, the grating feedback wavelength does not tune totally in phase with the cavity modes, which leads to the mode

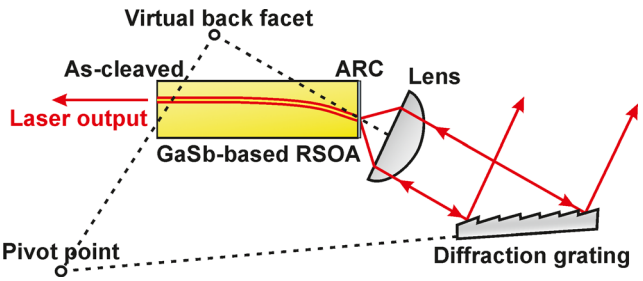

FIG. 3. Schematic of the Littrow laser.

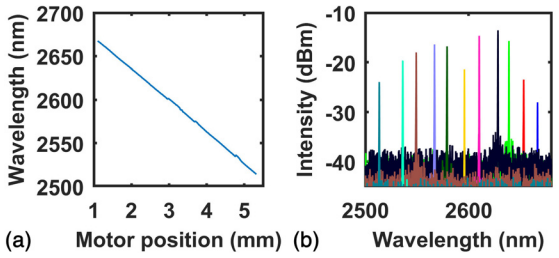

FIG. 4. (a) The emission wavelength of the Littrow laser as a function of the motorized actuator position and (b) emission spectra at different motorized actuator positions.

hops in the tuning curve. Mode-hop-free (MHF) tuning on the order of few nanometers around any wavelength is possible by adjusting the location of the pivot point or the injection current since this will change the cavity phase and subsequently the location of the external cavity modes.

Figure 4(b) shows emission spectra at different motorized actuator positions. The diffraction grating and collimation optics were aligned at 2.6 μm emission wavelength, and higher intensities at other wavelengths can be achieved by actively aligning the optics at each wavelength. The lowest spectral FWHM and the highest side-mode suppression ratio (SMSR) are reached when the cavity modes and the grating reflection wavelength overlap. Overlapping can be achieved at any wavelength value, e.g., by adjusting the pivot point position or the injection current. The lowest measured FWHM and SMSR values were $<$0.2 nm and $\sim$25 dB, respectively, and the measurement was limited by the resolution of the FTIR and the strength of the signal.

The maximum average output power was achieved at 2628 nm and is $\sim$10 mW with 1500 mA pulsed injection. This corresponds to a peak power of $\sim$100 mW. This is higher than what has been reported for Littrow lasers at 2.05–2.45 μm,[19] with comparable SMSR values. The lowest threshold current of $\sim$200 mA was also achieved at 2628 nm. The average output powers at 2513 nm and 2667 nm were $\sim$0.9 mW and $\sim$0.4 mW, respectively. The laser also produced mW-level power in CW operation. However, the highest average powers are achieved in pulsed operation, and we expect average powers several times higher than 10 mW to be achievable by optimizing the pulsed injection parameters.[18] This would result in similar power levels as reported for Littrow lasers at 2.05–2.45 μm,[19] with a wider tuning range and comparable SMSR. The power level would also be similar to Littman–Metcalf lasers reported at 1.7–2.5 μm,[20] although with a narrower tuning range and lower SMSR.

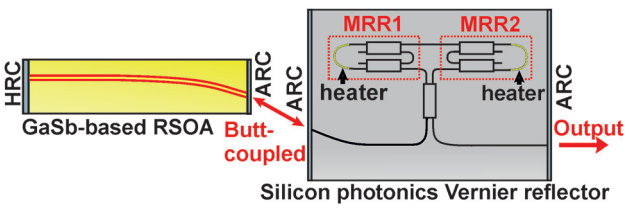

FIG. 5. Schematic of the Vernier laser, where the SiPh chip is used as the outcoupler.

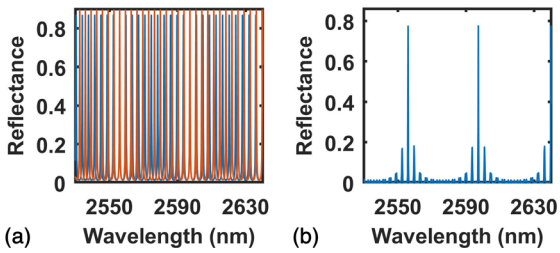

FIG. 6. (a) An example of a simulated reflectance spectrum from the individual MRRs (red: MRR1, blue: MRR2) and (b) the total reflectance.

In the Vernier laser, the RSOA was placed on a heatsink attached to a rotation stage, and the SiPh chip was placed on a three-axis stage. Both facets of the SiPh chip were AR coated to minimize parasitic reflections from the facets. Using rotation and three-axis stages, the waveguides in the RSOA and the SiPh chip were aligned by maximizing the output signal measured with a single-mode fiber (SMF) from the end-facet of the SiPh chip. A schematic of the laser is shown in Fig. 5.

The SiPh chip was fabricated at VTT and utilizes the 3 μm silicon-on-insulator (SOI) platform, which features low optical losses and the possibility for ultra-dense integration.[22] The chip consists of two MRRs (MRR1 and MRR2) with slightly different lengths, producing slightly different free spectral range (FSR) values. This will lead to Vernier effects, where only some of the reflectance peaks (spaced by a certain FSR value) overlap, while the other peaks are suppressed. The nominal lengths of MRR1 and MRR2 were 774.3 μm and 817.1 μm, respectively. An example of a simulated reflectance spectrum from individual MRRs and the total reflectance spectrum from such a reflector are shown in Fig. 6. Integrated next to the MRRs on the SiPh chip are two resistive heaters, allowing us to change the effective refractive index of the individual MRRs. Using the heaters, the wavelength of the laser can be tuned by controlling the voltage applied to them. The SiPh chip utilized 85:15 multimode interference (MMI) couplers, which couple $\sim$50% of the Vernier signal to the back to the RSOA and $\sim$50% of the signal into the output waveguide.

The Vernier laser was driven with 2 A pulses, and the output spectrum was scanned, while the drive voltages to the resistive heaters integrated on MRR1 and MRR2 were varied from 0 V to 20 V. Figure 7(a) shows the tuning map, where the x-axis shows the drive power to the heater integrated on MRR1, the y-axis shows the drive power to the heater integrated on MRR2, and the color shows the

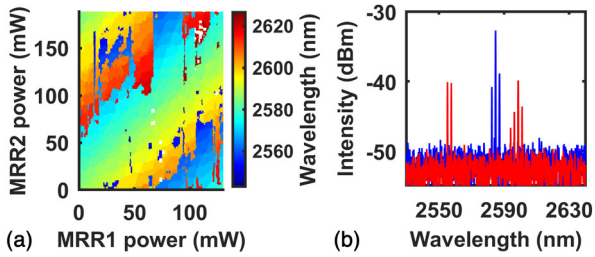

FIG. 7. (a) Emission wavelength (color) of the Vernier laser as a function of the power driven to each heater (x- and y-axes) and (b) emission spectrum at two operation points.

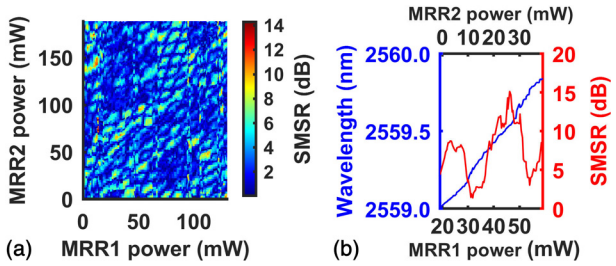

FIG. 8. (a) A map showing the SMSR (color) as a function of power driven to each heater and (b) demonstration of MHF tuning from 2559 nm to 2559.8 nm.

emission wavelength. The laser exhibits a wide tuning range of approximately 70 nm, with access to almost all wavelengths between 2550 nm and 2620 nm. The small mode hops of ∼2 nm arise from the FSR of the individual MRRs, while the large mode hops of ∼42 nm exist because the gain bandwidth of the RSOA is wider than the FSR of the SiPh reflector, leading to mode competition between adjacent Vernier reflector modes.

Figure 7(b) shows the emission spectrum of the laser at two operation points. The output power of the laser was in the μW-level. This relatively low value is due to waveguide coupling losses and losses of the SiPh chip (∼6 dB based on preliminary assessment). The spectral purity of the laser is limited mainly by two factors: (a) the limited FSR of the SiPh chip, which leads to emission around two reflectance peaks (red spectrum curve), and (b) the presence of side modes even when the laser is locked to one of the main reflectance peaks (blue spectrum curve). The issue (a) can be resolved by designing a SiPh chip with a wider FSR, which exceeds the gain bandwidth of the RSOA. The issue (b) is related to the fact that the reflectance of the peaks that are adjacent to the maximum reflectance is not low enough to suppress the modes. This can be solved by designing SiPh chips with more contrast between the reflectance values. In addition, the overlap between the cavity modes and the maximum reflectance is not optimal, which can be resolved by integrating a phase shifter into the SiPh chip. Additionally, a higher Q factor would decrease the probability of cavity mode overlap with the adjacent reflectance peaks.

Figure 8(a) shows the map of the SMSR as a function of the drive powers. The measurement was limited by the relatively poor signal-to-noise ratio (SNR) due to the low output power. There are regions where the SMSR reaches high values (around 14 dB at best), separated by low SMSR regions. We investigated one of these high SMSR value regions, and it was found that by tuning the heaters simultaneously near this region, quasi-continuous tuning could be achieved. Figure 8(b) shows tuning from 2559 nm to 2559.8 nm. True MHF tuning would require a

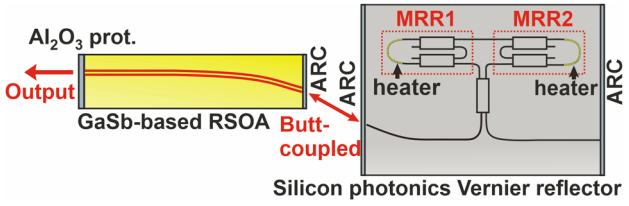

FIG. 9. Schematic of the Vernier laser, where the RSOA is used as the out-coupler.

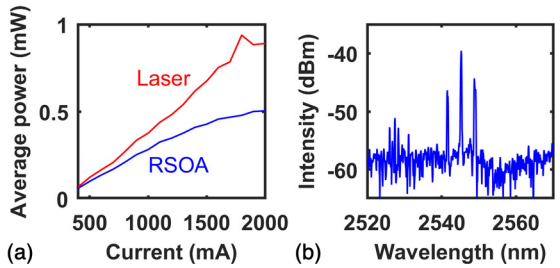

FIG. 10. (a) The average output power of the RSOA rear facet (blue) and the Vernier laser (red) as a function of injection current pulse amplitude and (b) the emission spectrum of the Vernier laser at 2000 mA.

phase shifter to be implemented into the SiPh chip, in order to tune the cavity modes in phase with the reflectance peaks.

Finally, a configuration in which the SiPh chip was used as an end mirror and the output was taken from the facet of the RSOA was tested, exhibiting a reflectivity of ∼30%. In addition, the SiPh chip utilized 72:28 MMI, leading to a stronger feedback of about 72%. The nominal lengths of MRR1 and MRR2 were 504.3 μm and 544.7 μm, respectively. The resistive heaters were not tuned in this configuration. A schematic of this configuration is shown in Fig. 9.

Figure 10(a) shows the average output power as a function of injection current for the RSOA without the SiPh chip (blue) and for the Vernier laser (red). Figure 10(b) shows the output spectrum at 2000 mA injection current, which shows lasing, although with clear side modes. The maximum average output power of the Vernier laser is obtained at 2000 mA, and it is ∼1 mW. This corresponds to a peak power of ∼10 mW, which is ∼10 times higher than what has been reported for similar lasers at 2.35 μm near RT.[17] The power is also several orders of magnitude higher than the power that was obtained when the Vernier reflector was used as the out-coupler. This confirms our estimation for the high losses in the SiPh chip waveguide coupling.

In conclusion, we have demonstrated a tunable GaSb/silicon extended-cavity laser in the 2.5–2.7 μm wavelength region, with record broad tunability from a single chip for such hybrid laser implementation at >2 μm.[10] The Littrow laser and the Vernier laser exhibited wide tuning ranges of 154 nm and 70 nm, respectively. While the average output power of the Vernier laser was limited to ∼1 mW, the Littrow laser demonstrates the excellent power capabilities offered by the GaSb-based RSOAs in a TDL configuration. On the other hand, the Vernier laser is much more attractive in terms of integration capability due to its compactness and lack of moving parts. Our future work will focus on optimizing the Vernier laser designs in terms of improving the waveguide coupling and designing SiPh chips with lower losses and wider FSR, which should lead to significantly higher output power and improved spectral purity, as well as a wider tuning range of more than 100 nm. When aiming at hybrid integration of tunable lasers, thick-SOI waveguides can be efficiently coupled to RSOA chips that are assembled in a cavity etched in the silicon chip. This has several advantages, including high-coupling efficiency, low-cost wafer-scale assembly, and miniaturized packaging.

The authors wish to thank M.Sc. Jarno Reuna for the preparation of AR/HR coatings and Ms. Mariia Bister for the

fabrication of the devices. S.-P. Ojanen would like to thank Vaisala Oyj for the funding of the Ph.D. program. The research was funded by EU H2020 project MIREGAS (Grant Agreement No. 644192) and Business Finland project RAPSI (Decision 1613/31/2018). This work is part of Academy of Finland flagship program PREIN (Decision 320168).

REFERENCES

[1]I. E. Gordon, L. S. Rothman, C. Hill, R. V. Kochanov, Y. Tan, P. F. Bernath, M. Birk, V. Boudon, A. Campargue, K. V. Chance *et al.*, J. Quant. Spectrosc. Radiat. Transfer **203**(Supplement C), 3 (2017).
[2]P. Werle, Spectrochim. Acta, Part A **52**, 805 (1996).
[3]T. Hu, B. Dong, X. Luo, T.-Y. Liow, J. Song, C. Lee, and G.-Q. Lo, Photonics Res. **5**, 417 (2017).
[4]R. Soref, Nat. Photonics **4**, 495 (2010).
[5]V. M. Lavchiev and B. Jakoby, IEEE J. Sel. Top. Quantum Electron. **23**, 8200612 (2017).
[6]T. Hosoda, T. Feng, L. Shterengas, G. Kipshidze, and G. Belenky, Appl. Phys. Lett. **108**, 131109 (2016).
[7]J. Viheriälä, K. Haring, S. Suomalainen, R. Koskinen, T. Niemi, and M. Guina, IEEE Photonics Technol. Lett. **28**, 1233 (2016).
[8]C. Lin, M. Grau, O. Dier, and M.-C. Amann, Appl. Phys. Lett. **84**, 5088 (2004).
[9]B. Liu, A. Shakouri, and J. E. Bowers, Appl. Phys. Lett. **79**, 3561 (2001).
[10]P. McNicholl and H. J. Metcalf, Appl. Opt. **24**, 2757 (1985).
[11]M. Faugeron, M. Tran, O. Parillaud, and M. Chtioui, IEEE Photonics Technol. Lett. **25**, 7 (2013).
[12]Y. A. Akulova, G. A. Fish, P.-C. Koh, C. L. Schow, P. Kozodoy, A. P. Dahl, S. Nakagawa, M. C. Larson, M. P. Mack, T. A. Strand, C. W. Coldren, E. Hegblom, S. K. Penniman, T. Wipiejewski, and L. A. Coldren, IEEE J. Sel. Top. Quantum Electron. **8**, 1349 (2002).
[13]R. Wang, S. Sprengel, A. Vasiliev, G. Boehm, J. V. Campenhout, G. Lepage, P. Verheyen, R. Baets, M.-C. Amann, and G. Roelkens, Photonics Res. **6**, 858 (2018).
[14]J. R. Meyer, C. A. Hoffman, and F. J. Bartoli, Appl. Phys. Lett. **67**, 757 (1995).
[15]T. D. Eales, I. P. Marko, B. A. Ikyo, A. R. Adams, S. Arafin, S. Sprengel, M.-C. Amann, and S. J. Sweeney, IEEE J. Sel. Top. Quantum Electron. **23**(6), 1 (2017).
[16]T. D. Eales, I. P. Marko, B. A. Ikyo, A. R. Adams, I. Vurgaftman, S. Arafin, S. Sprengel, M.-C. Amann, J. R. Meyer, and S. J. Sweeney, in Conference on Lasers and Electro-Optics Europe European Quantum Electronics Conference (CLEO/Europe-EQEC), Munich, Germany, 25–29 June (2017), p. 1.
[17]N. Zia, J. Viheriälä, E. Koivusalo, and M. Guina, Appl. Phys. Lett. **115**, 231106 (2019).
[18]N. Zia, J. Viheriälä, E. Koivusalo, H. Virtanen, A. Aho, S. Suomalainen, and M. Guina, Appl. Phys. Lett. **112**, 051106 (2018).
[19]I. Šimonytė, L. Andrulionis, J. Aleknavičius, G. Naujokaitė, E. Dvinelis, A. Trinkūnas, M. Greibus, A. Vizbaras, and K. Vizbaras, Proc. SPIE **10111**, 101110H (2017).
[20]A. Vizbaras, I. Šimonytė, S. Droz, N. Torcheboeuf, A. Miasojedovas, A. Trinkūnas, T. Bučiūnas, Z. Dambrauskas, A. Gulbinas, D. L. Boiko, and K. Vizbaras, IEEE J. Sel. Top. Quantum Electron. **25**, 1 (2019).
[21]M. Cherchi, S. Ylinen, M. Harjanne, M. Kapulainen, and T. Aalto, Opt. Express **21**, 17814 (2013).
[22]T. Aalto, M. Cherchi, M. Harjanne, S. Bhat, P. Heimala, F. Sun, M. Kapulainen, T. Hassinen, and T. Vehmas, IEEE J. Sel. Top. Quantum Electron. **25**, 1 (2019).